DIGITAL RECEIVER WITH INTERFERENCE SUPPRESSION FOR MICROWAVE RADIOMETRY

Final Report

Instrument Incubator Program Project NAS5-2001

Ohio State University Research Foundation Project 742068

Joel T. Johnson[*] and Steven W. Ellingson[†]

May 9, 2005

[*]Department of Electrical and Computer Engineering and ElectroScience Laboratory, The Ohio State University, 1320 Kinnear Rd., Columbus, OH 43212

[†]Bradley Department of Electrical and Computer Engineering, Virginia Tech, 302 Whittemore Hall, Blacksburg, VA, 24061

Contents

8 Conclusions   46

1 Introduction

This document serves as a final report for the project "Digital receiver with interference suppression for microwave radiometry" [1], supported under the NASA Instrument Incubator Program (IIP) from March 11th, 2002 to May 1st, 2005 at The Ohio State University ElectroScience Laboratory (ESL). The project goal was to develop microwave radiometer systems that include digital receiver-based RFI removal processing, so that RFI effects on microwave radiometers can be reduced. This is of particular interest for microwave radiometry at both L- and C-bands, given the strong RFI sources at L-band and limited protected spectrum (1400-1427 MHz), as well as the absence of protected spectrum at C-band. The IIP project focused specifically on L-band microwave radiometry, although the systems developed have also been applied for C-band observations in a related project [2].

Three digital receiver prototypes developed under the project are described in this report, along with the time- and frequency- blanking RFI mitigation algorithms implemented in these systems. Demonstrations of the prototypes in local observations, radio-astronomy measurements from the Arecibo radio observatory, and from an airborne platform at C-band are also discussed. An evaluation of the performance of the algorithms considered is provided, based on both local and airborne RFI surveys at L-band. Finally, issues related to deployment of these technologies in space systems are reviewed. Results show these systems to be excellent candidates for continued development for use in space designs; a proposal for the HYDROS L-band radiometer [3] has already initiated this process.

The next section provides a final administrative summary of the project, while Sections 3 and 4 provide an overview of RFI issues for microwave radiometry as well as the basic system concepts employed. A description of RFI survey efforts of the project as well as suppression algorithm evaluation efforts follows in Section 5, and results from several measurement campaigns are presented in Section 6. Issues for space deployment are then described in Section 7, and Section 8 presents final conclusions.

2 Administrative issues

2.1 Project dates

Although awarded in late 2001, contract negotiations between the Ohio State University Research Foundation and NASA GSFC selected a project start date of March 11th, 2002. Although typical IIP projects occupy a 36 month duration, delays in the negotiation process produced a reduced duration of 33 months (original end date 11/1/04). A request for a no-cost end-date extension to NASA from Ohio State was granted in 2004, resulting in the final project end date of 5/1/05.

2.2 Personnel

Ohio State University research personnel involved in the project have included:

- Assoc. Prof. Joel T. Johnson (PI)

- Asst. Prof. Steven W. Ellingson (co-PI) (Virginia Tech, formerly a research scientist at OSU until August 2003)

- Research Scientist Grant A. Hampson (System engineering) (joined CSIRO, Australia May 2004)

- Research Associate Rangarajan Krishnamachari (System engineering)

- Research Scientist Chi-Chih Chen (RF Support)

- Technicians Jim Moncrief and Ray Feast

- Graduate students David Wiggins (MS 6/02), Nakasit Niltawach (MS 6/03), Noppasin Niamsuwan (MS exp. 6/05)

- Undergraduate students Scott Orlove, Ryan Schultz, Ben Sensheimer, Miguel Lafleche, Mark Frankford

Among the graduate students, Noppasin Niamsuwan will complete his MS thesis in 2005 based upon material from the project [4]. Other graduate students provided support to the project but did not include project results in their theses.

2.3 Expenditures

The project budget included allocations of \$260,505 for year 1 (9 months), \$294,407 for year 2, and \$288,919 for year 3. This balance has been fully expended as of 5/1/05. Of the year 1 funds, \$21,000 was allocated to equipment for the purchase of a spectrum analyzer to assist in RFI survey studies. OSU provided cost-sharing to the project of \$10,885 for the equipment purchase, as well as approximately \$34,000 for cost-sharing of student tuition.

2.4 Publications

Several publications have resulted from project efforts included one journal article published [5], another accepted for publication [6], eight conference publications [7]-[14], and a NASA Tech Brief [15]. C-band studies with the digital backends developed have also been reported in a conference paper [16] and in a journal article currently in preparation. A website [17] has been created to archive internal project documents, including interim and annual review presentations [18]-[23]. The project has been maintained as publicly "open", and no patent disclosures have been filed given the public disclosure of all project efforts.

2.5 TRL levels and quad chart

Because digital receiver technologies had previously been applied to microwave radiometer systems (although not for RFI suppression in Earth-observations), the entry TRL rating for the project was taken as TRL 3 ("laboratory studies to physically validate predictions of separate technology elements"). The exit TRL level of the project can be taken as somewhere between 4 ("component and/or breadboard validation in laboratory environment") and 5 ("component and/or breadboard validation in relevant environment"), given the final experimental results that will be discussed in Section 6. It is estimated that completing the progression of these technologies to TRL 6 designs could be accomplished within a two- to three-year time frame, given the proposal to deploy these technologies in the HYDROS system, scheduled for launch in 2010.

6

A final quad chart for the project is illustrated in Figure 1; an electronic copy of this chart is available at the project web site [17].

3 RFI issues for microwave radiometers

The design of a traditional microwave radiometer is based on the assumption that the observed signal consists only of thermal noise. Because the goal of radiometry is to estimate accurately the mean power of the incoming thermal noise, long integration periods (on the order of milliseconds or longer) are desirable in order to reduce uncertainty. Only the mean power estimate after this integration period is of interest, so a traditional radiometer will not record information within an integration period. In addition, the use of large bandwidth channels is desired in order to further reduce uncertainty in the estimate of mean power. Because naturally emitted thermal noise varies very slowly with frequency in most cases, measurements from channels with similar center frequencies are deemed identical, and single channel observations are sufficient to represent a large portion of the spectrum.

A traditional "direct detection" radiometer block diagram is illustrated in Figure 2; the front end filter here typically includes a large bandwidth (10's or 100's of MHz), while the low pass filter integrates the power up to millisecond scales before digitization.

The addition of RFI to the observed channel violates the noise-only assumption, and causes serious problems for a traditional radiometer. Although interference can take a variety of forms, in many cases RFI may be expected to be localized either in time (i.e. pulsed type interference) or frequency (narrowband interference), or in both domains. If only a small number of such "localized" interfering sources are present, a large portion of either the observation time or bandwidth may contain no interference. However, the traditional radiometer is unable to separate the corrupted and uncorrupted portions of the observation, and therefore may produce corrupted data even with only limited RFI. Because RFI will always increase the mean power when compared to that of the geophysical background, post-processing of the data can be applied to eliminate abnormally high observations. However, lower level RFI

Digital Receiver With Interference Suppression for Microwave Radiometry

PIs: Joel T. Johnson (Ohio State) and Steven W. Ellingson (Virginia Tech)

Objectives

- Future sea salinity and soil moisture sensing missions use L-Band microwave radiometry
- RF interference is a major problem and limits useable bandwidth to 20 MHz.
- An interference suppressing radiometer could
  - reduce RFI effects on these systems
  - allow operation in a larger bandwidth for more accurate moisture/salinity retrievals
- Project developed a radiometer digital backend including real-time removal of time and/or frequency localized RFI sources
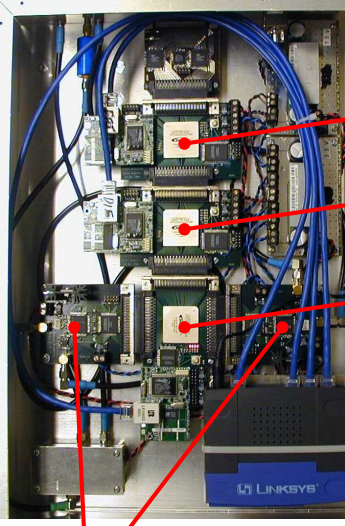
200 MSPS 10 bit ADC's

Implemented in Altera FPGA's

Real-time "pulse blanking" algorithm

1K FFT = high spectral resolution RFI removal

Spectral proccessing/ integration

1K FFT

Digital filtering/ pulse blanking

Accomplishments

- Receiver prototypes developed; sample 100 MHz bandwidth with real-time pulse blanking and 1K FFT
- Demonstrated at Arecibo radio observatory and in local observations of water pool and sky targets
- Results qualitatively show significant RFI mitigation and advantages of high spectral resolution
- RFI surveys at L-band (including airborne measurements) completed under project support
- System developed can be applied in other RF bands: NPOESS sponsored project using this system at C-band in progress: results to influence CMIS design
- Proposal to utilize these technologies at L-band in the HYDROS program under evaluation

TRL_{in} =3; TRL_{out} =4

Project URL: http://esl.eng.ohio-state.edu/~rstheory/iip/docserv.html
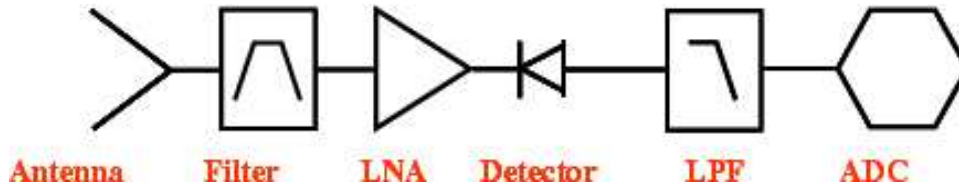
Figure 1: Final project quad chart

Figure 2: Block diagram of traditional radiometer system

can be difficult to separate from geophysical information, making parameter retrievals problematic. Note that an interferer with a large amplitude but small temporal duty cycle and/or small bandwidth may appear as low level RFI when averaged over time and frequency.

A simple way to extend the RFI mitigation capabilities of the traditional radiometer is to increase either the temporal sample rate or the number of frequency channels in the system. These approaches can be implemented in an analog fashion by simple extensions of the traditional radiometer, and the complete data set recorded for post-processing to eliminate RFI at finer temporal and spectral resolution. However, the number of channels that can be implemented using an analog approach is limited, given that additional hardware must be added for each new channel. The temporal sampling rate that can be achieved is also limited by both the RF hardware and the data acquisition subsystem, since the amount of data to be stored eventually becomes unmanageable. Use of digital receiver technologies can address some of these issues: the implicit high temporal sampling rate of a digital receiver allows temporally localized sources to be resolved. In addition, an FFT operation can be performed in real time to obtain a much larger number of frequency channels than is possible using analog sub-channels. However, the data rate of such a system is also much larger than that of the analog approaches. To reduce the data rate, an RFI mitigation processor can be added to the digital receiver to implement simple time and/or frequency domain mitigation algorithms in real time. The resulting "RFI-free" data is then

integrated over time and/or frequency to produce a manageable final output data rate.

The digital receiver developed under the IIP project is based on such an architecture. Figure 3 illustrates this configuration; note a downconversion stage is included given that directly sampling the incoming RF energy may be difficult due to analog-to-digital converter (ADC) limitations. Direct RF sampling has been utilized in L-band radiometry previously [24], but the receiver prototypes developed in the current project include downconversion stages.
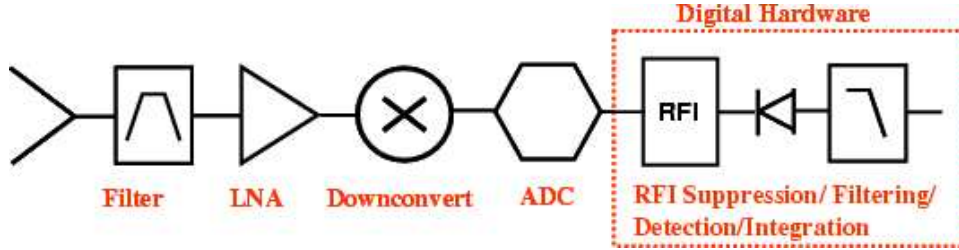
Figure 3: Block diagram of new radiometer system

4   System overview

Figure 4 presents a more detailed block diagram of the microwave radiometer system developed [25]-[26]. The basic design consists of a standard radiometer frontend, an analog downconverter section, and a digital backend unit capable of coherently sampling a 100 MHz bandwidth. A bandwidth of 100 MHz was chosen for the system based on a compromise between available digital technology and a desire for large bandwidth operations. At L-band, this bandwidth includes the 20 MHz of protected spectrum, as well as other spectral regions more likely to contain RFI sources. The same digital backend system (i.e. after the downconversion stage) can be utilized at an arbitrary RF frequency simply by modifying the antenna, front end, and downconversion stages.

Figure 4: Block diagram of radiometer

It is desirable to include a large number of bits in the sampling process in order to resolve both environmental noise and RFI contributions without encountering dynamic range problems. A survey of available ADC's at the beginning of the project [27]-[29] showed that a sample rate of 200 MSPS (so that 100 MHz is the maximum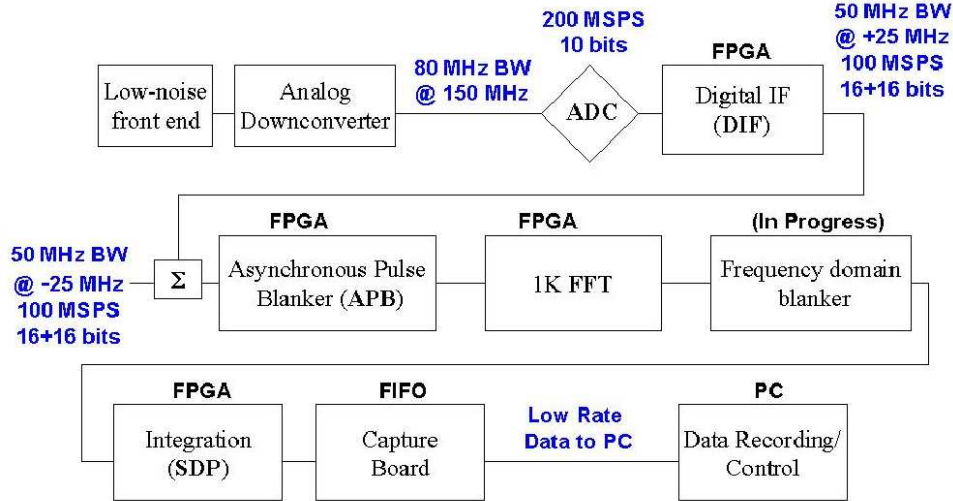 bandwidth resolvable) with 10 bits was the limit of easily available technology as of early 2002. Using a large number of ADC bits opens the possibility of reduced gain in the radiometer frontend and downconverter sections, as higher dynamic range is typically achieved in ADC's by increasing sensitivity (i.e. lowering the power required to toggle the lowest ADC bit.) Reduced gain is desirable in general in order to improve receiver stability, and thereby potentially reduce thermal control requirements throughout the entire system. Trade-off studies of receiver stability versus gain were not performed under the IIP project however.

Although resolving 100 MHz with one such ADC would be possible, it was deemed preferable to utilize 2 ADC's sampling 50 MHz each so that digital filtering could be incorporated into the RFI processor to limit receiver bandwidth digitally. Use of digital filters is desirable due to possible stability issues of analog filters with temperature and other environmental variations, particularly near the cutoff frequencies of the filter response. The design developed keeps the analog filter passband wider than

11

that ultimately set by the digital filters, so that the near cutoff regions of the analog filters do not contribute significantly to the observed bandwidth.

Accordingly, the 100 MHz bandwidth is split into 2 50 MHz channels, and each channel is then sampled at 200 MSPS using 10 bits. The resulting digital data of each channel is centered at 50 MHz and is spectrally reversed due to the use of the second ADC Nyquist zone. The "Digital IF" (DIF) FPGA module downconverts each channel to 0 Hz (so now the samples are complex-valued), digitally filters each to 50 MHz bandwidth, decimates by 2, and then up- or down-converts the two channels to center frequencies of +/-25 MHz (still complex). Finally both channels are added so that -50 to 50 MHz data emerges from the DIF module in 16-bit "I"+16-bit "Q" format at 100 MSPS. See [25] and [30]-[32] for a more detailed description of the digital IF section.

Following the DIF output is a cascade of FPGA modules which can be programmed to perform a variety of functions. The strategy used in the current project is as shown in Figure 4: mitigation of radar pulses using "asynchronous pulse blanking" (APB), channelization into 100-kHz bins using a 1K FFT, and integration to generate power spectra.

The APB [33]-[34] is designed to detect and blank radar pulses, which often are the dominant source of external L-Band RFI below 1400 MHz. Typical radar pulses range from 2-400 μs in length and occur 1-75 ms apart [35], illustrating the low temporal duty cycle of these sources. To detect these pulses, the APB maintains a running estimate of the mean and variance of the sample magnitudes. Whenever a sample magnitude greater than a threshold number of standard deviations from the mean is detected, the APB blanks (sets to zero) a block of samples beginning from a predetermined period before the triggering sample, through and hopefully including any multi-path components associated with the detected pulses. APB operating parameters are adjustable and can be set by the user. Operation of the APB is described in more detail in Section 4.1.

Following the APB is a length-1K complex FFT [36]-[37], which achieves approximately 98% duty cycle in performing the FFT computations. A triangular window

[38] is applied before the FFT. Considered but not implemented in the hardware of this project is a frequency domain blanking module, which is similar in concept to the APB, except applied independently to each frequency bin; frequency domain blanking is discussed further in Section 4.2. The FFT output is processed through a "spectral domain processor" (SDP) module which computes the magnitude-squared for each frequency bin [39] and computes a linear power average over many FFT outputs [40]. Calibration corrections for the blanking operation are incorporated by recording the number of blanked samples included in an SDP integration period. The SDP module is also capable of computing a max-hold operation in RFI detection applications. Results from the SDP are passed at a relatively low rate to a PC via a "capture" interface system [41]. Total power can be computed by summation of frequency bins within the digital hardware, or the same process can be implemented in software for increased flexibility in removing RFI across frequency.

4.1 Pulse blanking

The detailed design of the APB system is described in [33], and its implementation in FPGA hardware is detailed in [34]. A study of APB parameters is also provided in [6]. As stated previously, the APB processor maintains a running estimate of the mean and variance of the time domain power following the DIF processor. When a incoming time-domain sample exceeds a threshold number of standard deviations from the mean, a blanking operation is initiated. This threshold (referred to as β) is the first parameter of the APB processor. Figure 5 illustrates an example time series of data in terms of its relative power, and includes samples that exceed a specified threshold value.

Once a blanking process is initiated, it is desirable to blank (i.e. set to zero) not only the "trigger" sample that exceeded the threshold value, but also samples preceding and following the trigger, as these samples likely contain RFI as well. Two additional parameters of the APB then result: a blanking window width (called $NBLANK$), and a parameter ($NWAIT$) related to the number of samples preceding the trigger that will be blanked. Note this process requires an internal memory in

order to be able to blank samples preceding the trigger sample; the system developed includes a 1K memory (representing 10.24 μsec of data given the 10 nsec sample spacing).
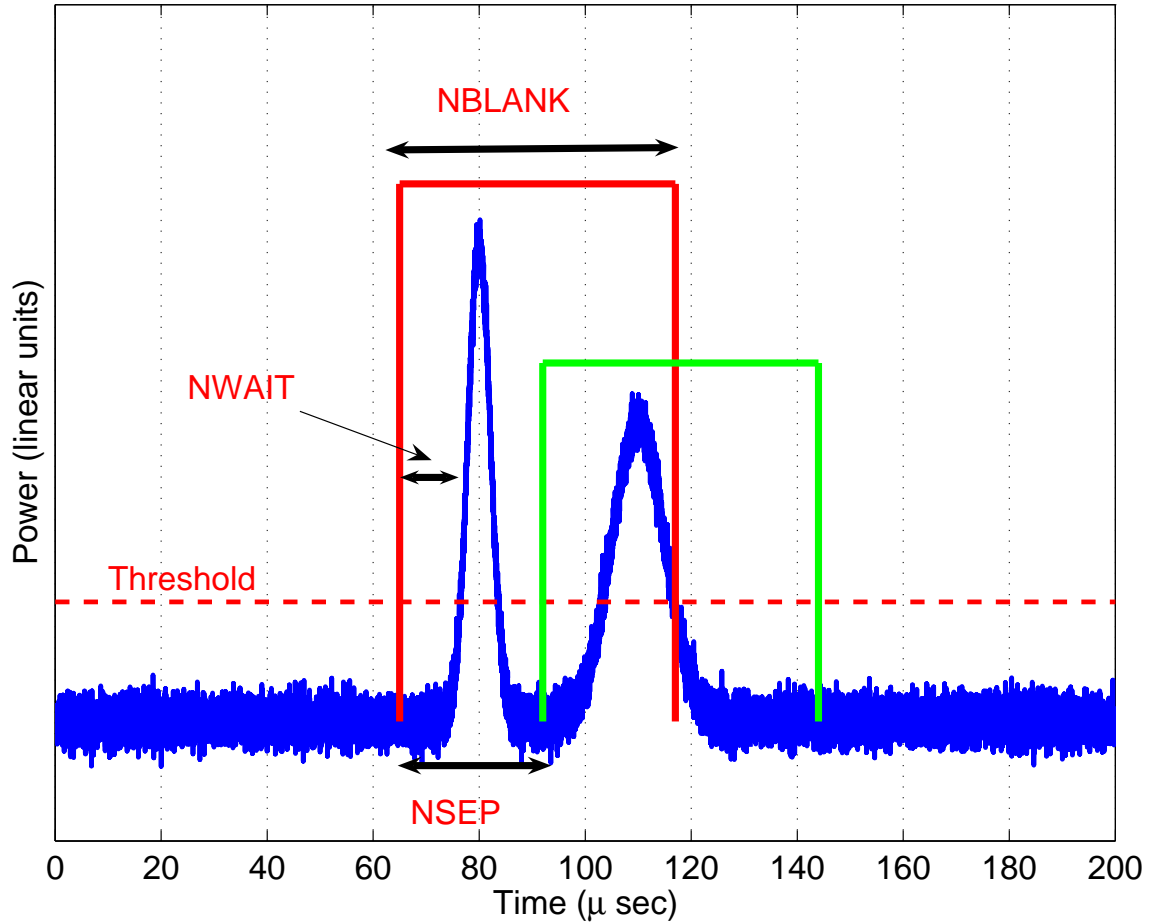
Figure 5: APB functional diagram: Relative power versus time

Figure 5 also illustrates that it is desirable to have the ability to initiate a second blanking operation during the time that a first blanking operation is being performed. The figure demonstrates a case in which a second RFI pulse is received near the end of the blanking operation for a first pulse. Note the second pulse exceeds the detection threshold only within the period of the first blanking operation, and does not exceed the threshold after the first blanking operation has completed. If no second blanking operation were initiated, the lower level RFI contributions of the second pulse which do not exceed the detection threshold would be allowed to remain

14

in the data. However a second blanking operation initiated during the period of the first blanking operation continues blanking to remove all second pulse contributions.

A final parameter of the APB processor arises due to the need for internal state machines to control each blanking process. These state machines are referred to as "blanking timing registers" (BTR's) in what follows. Because it is not possible to have an unlimited number of BTR's within the system, the possibility arises that all BTR's will be occupied performing blanking operations at some point in time, leaving no BTR's available to initiate a new blanking process when a particular sample exceeds the detection threshold. It is clear that an unlimited number of BTR's is not necessarily needed as well, if the limit of several successive samples exceeding the threshold is considered. Because the blanking operation typically blanks several samples when initiated, there is no need to have blanking operations initiated on successive detected samples occurring within a short time of each other. For this reason, it is desirable to introduce the $NSEP$ parameter, which determines the minimum allowed time delay between blanking process initiations. It is shown in [6] that appropriate choices of APB parameters can be made for a given number of BTR's so that all detected samples exceeding the threshold level are guaranteed to be blanked. The final prototype implementation included 4 BTR's.

Note that the blanking operation replaces the blanked data with zero; clearly this modification results in a change in the integrated total power eventually obtained by the radiometer. However, this change is easily corrected if the number of blanked samples (N_b) within the total number of integrated samples (N_t) is known: the average obtained is multiplied by a scaling factor $N_t/(N_t - N_b)$ to correct for blanking. This "APB counter" operation is included in the final system prototype developed. Blanking operations also influence computation of the FFT; this will be discussed in the next section.

With regard to the implementation of the APB processor achieved, a set of hardware issues were encountered. First, it was deemed important to retain full dynamic range in the estimation of the variance of the incoming power. This quantity involves the incoming field to the fourth power, resulting in a large number of bits needed in

detector arithmetic operations. This large number of bits slowed the APB detection processor significantly, so that it was able to operate only at one quarter the data rate of the incoming samples. A simple decimation-by-four procedure was utilized (i.e. the APB detection processor observed only one out of four incoming samples) to retain the APB system in the FPGA hardware developed. This is not expected to be a major limitation, as the bandwidth of likely pulsed RFI sources is not expected to exceed a few MHz, still much smaller than the 25 MHz rate of the final APB processor. Future revisions of an APB design can consider the alternative of reduced accuracy (i.e. bit widths) in detector processor computations in order to achieve increased speed.

A second hardware issue involves the desire to modify APB parameters (i.e. β, $NBLANK$, etc.) without the necessity of reprogramming the FPGA. An ethernet interface to the APB FPGA from a controlling computer was developed (through use a commercial microcontroller part) so that APB parameters can be modified as the system operates. The potential for adaptive modification of these parameters on a slower time scale (i.e. order of seconds) results, in order to optimize system performance as the RFI environment is varied. The ethernet interface also allows the APB blanking operation to be turned on or off, so that its influence can be observed on measured data.

4.2 Spectral RFI Processing

As stated previously, following the APB processor, a 1024 point FFT (with an optional triangular window before the computation) is performed. Use of the FFT provides high spectral resolution for resolving narrowband RFI sources; each channel is approximately 100 kHz wide, and the large number of channels obtained is beyond the expected capabilities of analog sub-channel methods.

4.2.1 Blanking effects on FFT spectra

Given FFT computation of "frames" that may contain blanked data, the possibility of corruption of the obtained FFT spectrum must be considered. Clearly frames con-

taining no blanking and those completely blanked yield no problems, while partially blanked frames will produce spectra that are convolved with the transform of the on/off pattern of the blanker. In the system developed, the APB blanking width is typically 40μsec, much longer than the 10μsec FFT frame width, so that a minimum of two completely blanked frames are obtained for each pair of partially blanked frames. Reference [6] explores the impact of the partially blanked frames in several studies, and shows their effects on distortion of the final output spectrum to be minimal for long integration periods. This is because FFT frames that produce the most distorted spectra are also those that are most blanked, resulting in a reduced power level for their contributions when included in the average power computation. The "slow scaling" procedure of APB calibration corrections (i.e. corrections implemented on the time scale of the radiometer integration period) is consistent with this insight.

4.2.2 Post-FFT RFI removal

Two types of simple post-FFT RFI suppression can be envisioned: cross-time and cross-frequency. The cross-time approach is identical to the APB algorithm but now applied to each FFT output bin. This results in a higher signal-to-noise ratio detection of interference localized in time and frequency. Note the temporal rates now considered are much slower than those of the original APB processor, as 10.24 μsec is required for each FFT computation. Although this system is a relatively straightforward extension of the APB processor, no attempts were made throughout the project to implement such an approach in hardware. This is because narrowband RFI (within a 100 kHz bin) following the APB processor is not typically expected to vary on μsec time scales, eliminating an immediate need for implementation in hardware. Implementation of the per-bin APB algorithm has been performed in software, and utilized to further remove short-time duration sources within individual FFT bins. Calibration corrections for blanking are similar to those employed for the original APB algorithm.

In contrast, cross-frequency blanking involves comparisons of results in different frequency bins, in order to detect and remove more time continuous RFI sources.

17

Again the long time scales expected for sources in this process did not motivate immediate consideration for implementation in hardware. A simple software based algorithm has been developed and utilized based on thresholding the derivative of the data in frequency. It is not immediately desirable to place a simple threshold on the raw power measured, as without calibration this is sensitive to possible variations over time of the instrument gain pattern versus frequency. This is important because if such an algorithm were implemented in hardware, it is unlikely that calibrated data would be utilized in the algorithm. The algorithm developed was also enhanced to incorporate information from the cross-time post-FFT algorithm in order to improve detection of corrupted FFT bins. Calibration corrections for cross-frequency blanking again are simple to implement, involving simply scaling by the number of frequency channels retained relative to the original number of channels. Note at L-band that high spectral resolution is useful in removing contributions from hydrogen line emissions at 1413 MHz, as these narrowband contributions can influence the accuracy of sea salinity retrievals from space [42].

4.3 Data rate issues

The goal of the IIP radiometer is to demonstrate real-time RFI suppression while maintaining a reasonable output data rate. While the system developed achieves this goal with regards to suppression of temporally-localized RFI (internal samples at 10 nsec, output samples at millisecond to second time scales), suppression of frequency localized RFI remains in software, resulting in a requirement to store 1024 frequency channels as opposed to a single channel. Implementation of the cross-time and cross-frequency blanking algorithms in hardware would solve this problem; however for the purposes of the IIP project this data rate was manageable and retained so that high resolution information on RFI spectral properties was archived. The dataset archived also allows software experiments with varying cross-time and cross-frequency post FFT techniques to be performed.

Given the fact that microwave radiometers typically have extremely low data rates compared to other systems onboard remote sensing satellites, an increase in data

rates beyond those of previous systems may be acceptable, allowing space systems to retain flexibility in cross-frequency RFI removal methods. In fact the CMIS sensor of NPOESS already plans to include 4 C-band sub-channels, with RFI removal in these channels accomplished in post-processing. Although use of 1024 channels may exceed practical limitations for space operations, use of 16 or even 32 channels is likely to be feasible, making the software based algorithms developed relevant for application to space-based systems.

4.4   Receiver prototypes developed

Over the course of the project, three prototype digital receivers have been completed; photographs of these receivers are available in [23]. The first, LISR1 [40], included only one ADC and therefore sampled only a 50 MHz bandwidth, but retained the full DIF, APB, FFT, and SDP operations with a few exceptions. Development of a system clock module for LISR1 is described in [43]. The FPGA components utilized in this prototype also were insufficient in size to allow a full duty cycle FFT operation. This resulted in only a 14% duty cycle for the final observations. LISR1 also included only one BTR, no APB calibration corrections, and no possibility of max-hold computations. LISR1 was completed by late September 2002, and was utilized in the Arecibo observation campaign discussed in Section 6.1.

A second prototype, LISR2 [44], was developed to remove the limitations of LISR1; Figure 6 is a photograph of the LISR2 digital backend. LISR2 included both ADC components, so that full 100 MHz observations were achieved. A higher-density series of FPGA components were also used (the Altera "Stratix" line), allowing parallel FFT processors to be included so that 98% duty cycle computations resulted. The LISR2 FPGA program was improved to include 4 BTRs as well as the max-hold operation. However, the APB scaling operation still remained difficult with LISR2 due to the presence of the APB and SDP components on separate FPGA cards. The ethernet interface to LISR2 allows operation of the system in several modes, including a direct recording of raw sampled ADC data, power integration with the APB on or off, as well as max-hold operations with the blanker on or off. LISR2 was completed by late
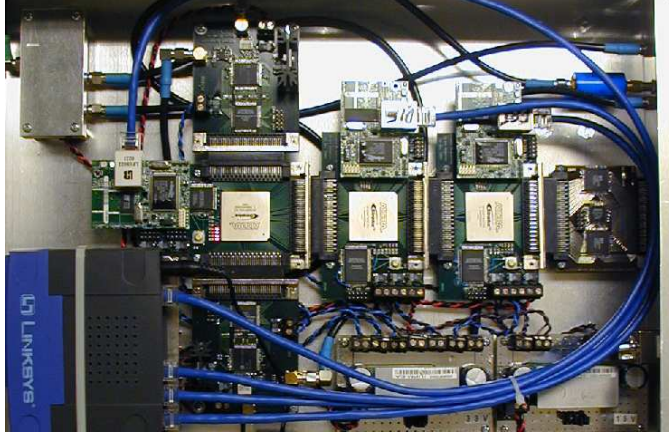
Figure 6: LISR2 digital backend; the vertical cascade of three circuit boards near the left hand side contains the dual ADC sections (upper and lower boards) and the digital channel combination and filtering (DIF) section (center board). The APB section for removing temporal pulses is also implemented on the center board. Following the vertical cascade to the right is the FFT processor, then the SDP section for power computation and integration operations. Finally a "capture card" provides the interface to the PC. Microcontrollers are also included on each card (the smaller attached circuit boards with ethernet cables) to enable PC setting of FPGA parameters through an ethernet interface.

April 2003, and utilized in local pool and sky observations, as well as in airborne observations at C-band.

A final prototype, LISR3, was developed to improve communication among separate components (i.e. DIF, APB, FFT, SDP) of the system. In particular, the APB calibration correction requires use of APB blanking information in the integration computation. A larger "Stratix" component was chosen to allow the entire processor to reside within a single FPGA. The large size of the program on this FPGA made simulation and programming difficult, and several studies involving use of dedicated FPGA registers as well as low-level signal routing were required in order to achieve an operational program. LISR3 was completed by late March 2005 (near the project end date) but enabled accurate APB calibration corrections to be achieved.

5   RFI surveys, LISA campaign, and algorithm testing

5.1   Local RFI surveys

A crucial aspect of system testing involves the RFI environment in which the tests are performed. Local tests at The Ohio State University ElectroScience Laboratory experience L-band RFI sources in the local region, so understanding these sources was important for monitoring performance. Accordingly, analytical [45] and measurement [46]-[48] studies of the local RFI environment were performed in 2002. Results showed a relatively quiet spectrum in the region 1325-1425 MHz, although a strong pulsed interferer was identified. This interferer is an air-route surveillance radar (ARSR), transmitting pulses of approximately $1\mu sec$ duration every 3 msec, located approximately 43 km from the laboratory in London, OH. This source provides an excellent pulsed interferer for assessing APB performance in local measurements. Additional more-continuous narrowband RFI sources have also been observed in the local environment; see [23] for data illustrating these sources.

5.2   LISA

Although the local OSU environment is likely somewhat representative of other ground-based L-band RFI environments, it was decided early in the project period through discussions with GSFC personnel (in particular Dr. Ed Kim) that airborne L-band RFI surveys in a variety of environments would be highly desirable. Such surveys could provide data for evaluating RFI mitigation algorithm performance against a larger set of sources than those experienced locally. In addition, it is to be expected that RFI power levels are larger in airborne than in ground-based observations, due to more rapidly increasing path loss encountered for ground-based versus free-space paths.

Through coordination with Dr. Kim, the L-band Interference Surveyor/Analyzer (LISA) was developed as part of the IIP project to perform these observations [49]-[56]. Because the first deployment of LISA occurred early in the project (January

2nd, 2003), it was necessary to develop the LISA system based on digital receiver designs already in existence early in the IIP project period. For this reason, LISA was based on a digital receiver capable only of sampling a 20 MHz bandwidth, and with no on-board RFI processing. However, the raw "capture"data recorded by LISA was ideal for further use in RFI suppression algorithm evaluations. An antenna-front end system, downconversion unit, and interface to a computer were all implemented for airborne observations.

LISA was deployed in a test flight onboard the NASA P-3 aircraft over the Chesapeake bay region on January 2nd, 2003, followed by a cross-US flight to Monterey, CA on January 3rd. A photograph of the LISA equipment rack on the aircraft is provided in Figure 7. LISA then was operated throughout transit to and in the AMSR-E Wakasa Bay cal-val campaign. LISA successfully recorded a large data set of RFI observations tuned throughout the 1300-1700 MHz band. Numerous RFI sources were observed and categorized, as described in [55]-[56]. Unfortunately, the sensitivity of the LISA system was limited due to placement of its antenna in the tail radome of the P-3 aircraft, so that no conclusive information on RFI in the L-band protected spectrum was achieved. However the large data set and variety of RFI environments experienced enabled a more general study of RFI mitigation methods to be performed.

5.3   Algorithm studies with LISA data

A particular emphasis of the LISA data studies involved performance of the APB algorithm. This algorithm was simulated in software on the LISA capture data, with the simulation code developed to mimic the hardware system behavior as much as possible. Several studies of the algorithm were performed, including tests of the Gaussianity of the data pre- and post-blanking, effects of variations in the APB threshold and blanking window width, as well as the influence of partially blanked frames in the FFT computation. Results of these studies are documented in [6]. These studies resulted in the "slow scaling" calibration correction procedure utilized in the LISR3 system, as well as improvements in parameter choices for later APB operations. The dataset remains available for future analyses of any new algorithms.

Figure 7: The LISA equipment rack installed on the P-3.

6   System demonstrations

Several demonstrations of the IIP system were performed throughout the project period, involving use of the LISR1, 2, and 3 prototypes. The majority of these observations recorded integrated FFT power outputs measured with the APB processor either on or off. The resulting data can be plotted as a "spectrogram" series, in terms of the power in all 1024 FFT bins versus time. For raw measured data, it is typical to normalize such plots by the average of each bin over time, so that the passband response of the instrument is removed.

Calibration of recorded data in microwave radiometer observations is based on the use of known brightness calibration targets [57]. Such targets ideally are external to the system antenna, so that the influence of all system components including the antenna can be accounted for in the calibration process. Because external calibration requires moving either the target or the antenna so that the antenna observes the calibration target, it is difficult to perform external calibration repeatedly within a short duration of time. However, receiver gain variations over short periods of time can occur that reduce the calibration accuracy of the system in-between external calibrations.

To address these shorter time scale variations, it is typical to include internal calibration sources within microwave radiometer systems as well. These internal loads (noise diodes with known emitted power levels, or microwave terminators at a known physical temperature) serve as standards for correcting receiver gain variations following to the location of the internal loads. Including a switch for internal load measurements as close to the antenna as possible is therefore desirable, so that the internal calibration corrects the majority of later system gain variations. However an internal calibration does not yield correct brightness values for antenna measurements, since the antenna response is not included in the correction.

The experiments to be discussed utilized a variety of calibration methods, including observation of raw data only in some cases. Unfortunately a completely calibrated set of observations at L-band was not achieved during the project period; airborne

observations at C-band however have yielded a small set of calibrated data, as will be discussed in what follows.

6.1 LISR1 measurements

Early local tests of the LISR1 system using a low gain antenna and interim front-end/downconverter stage are described in [40], [58]-[59]. These tests were completed by September of 2002, and provided uncalibrated tests of the capture, FFT, and integration stages of the LISR1 processor. The results qualitatively indicated the success of the APB processor at reducing contributions from the local ARSR system. In addition, tests with a terminated antenna input demonstrated the expected reduction in measured noise variances with integration times up to approximately 10 seconds, showing that the LISR1 digital processor achieved excellent performance as a radiometer subsystem over these time scales. Stability tests beyond this time duration were not appropriate in these measurements due to the absence of any temperature control and/or internal calibration loads in the tests. However the results clearly demonstrated that the digital backend processor functioned as designed, and that proceeding to the LISR2 development was appropriate.

An opportunity arose in November 2002 to co-observe with the LISR1 digital backend at the Arecibo radio observatory. Results from these observations are described in [5], [11], and [60]. The front-end and downconversion stages of the Arecibo observatory were used, and no information on an appropriate calibration procedure was available at the time of the measurements. For this reason results again are considered in terms of relative power variations only. Data were collected in the bands 1230-1280 MHz, 1275-1325 MHz, and 1325-1375 MHz (tuned throughout the campaign), using the "capture" mode (i.e. recording of raw ADC samples) as well as integrated data with the APB on or off. Due the presence of several radar systems in the Arecibo vicinity, the APB was again qualitatively shown to have a significant impact on reducing RFI in the dataset. Figure 8 illustrates integrated power levels in the band 1325-1375 MHz obtained from 10.7 seconds of LISR1 observations at Arecibo; the upper plot includes data with the APB off, while APB-on results are
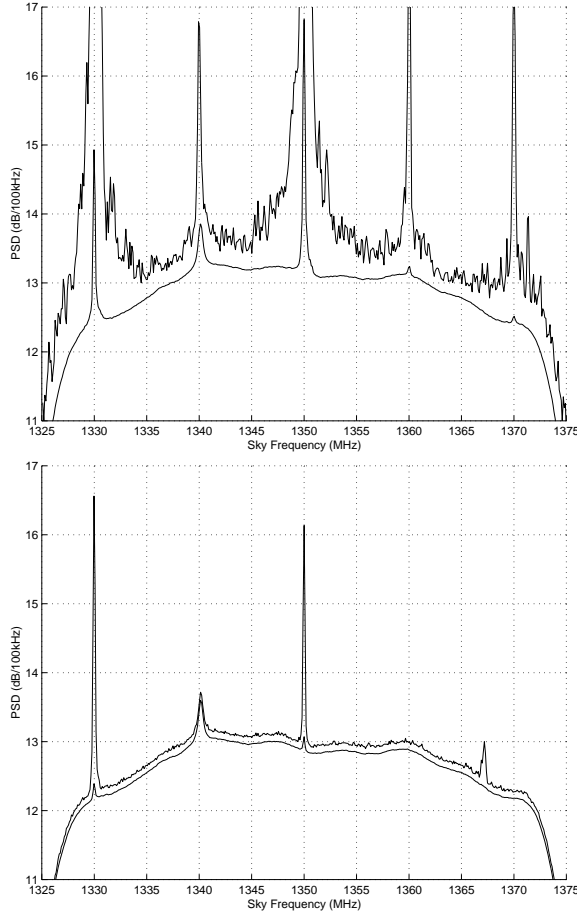
Figure 8: Sample mean and max-hold spectra from LISR1 observations at Arecibo. See [5], [11], and [60] for more information. *Top Panel:* APB off; *Bottom panel:* APB on.

shown in the lower plot. In addition, the upper curve within each plot is the maximum value for each FFT bin observed during the integration period; the lower curve is the average of all values. Clearly the APB system is dramatically reducing the impact of interferers at 1330 and 1350 MHz (known to be radar sources), especially in the maximum values observed. A detailed study of the capture data and properties of one of the radar sources observed is documented in [5].

6.2 LISR2 Pool campaign

6.2.1 Experiment design and system hardware

In order to obtain calibrated brightnesses in a local test, a well defined external calibration procedure is necessary. In addition, a true test would involve three well
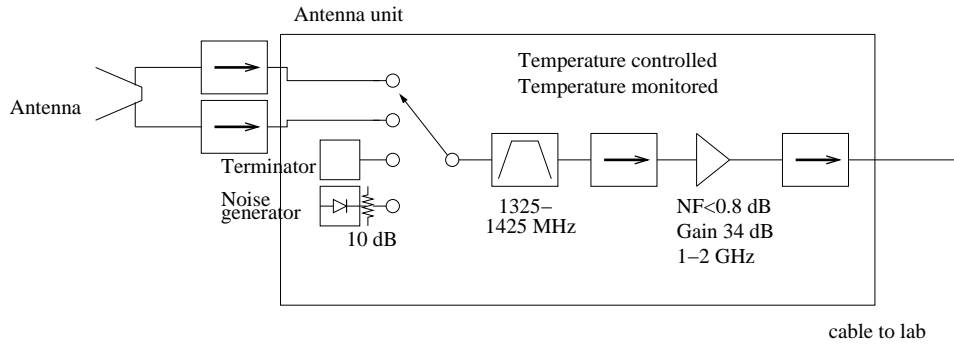
Figure 9: Block diagram of antenna/front-end unit developed for pool observations

characterized targets, with the first two targets defining the calibration and the third target being used to evaluate the accuracy of the calibration. It is also desirable to operate such an experiment in the antenna far-field, in order to avoid any complex behaviors of the antenna pattern with range in the near field. An experiment was designed to fulfill these needs involving observations of a large water pool with an antenna on the roof of the ElectroScience Laboratory building. Description of the experiment plan is provided in [57], [61]-[62].

Based on both geometric and far-field considerations, a 1.2 m reflector antenna was selected for the tests. This resulted in a wide antenna pattern, so that filling the antenna pattern completely with the calibration targets was not possible. An alternate approach was pursued based on calibrating only a portion of the antenna pattern, with the remainder of the antenna temperature being considered as system noise. Of course, the stability of this external noise over time is important if an accurate calibration was to be achieved. An antenna and feed were designed, along with appropriately sized water pool and calibration targets (microwave absorbers and reflectors) [63]. An integrated front-end [64]-[66] was also designed for this antenna, including switched observations of internal noise diode and terminator sources, as well as both horizontal and vertical polarizations of the antenna. Figures 9 and 10 are block diagrams of the final front-end and downconversion units used, respectively. A photograph of the reflector, feed, integrated front-end unit, and antenna mount is provided in Figure 11. These systems along with the external targets were developed during the Spring and Summer of 2003.
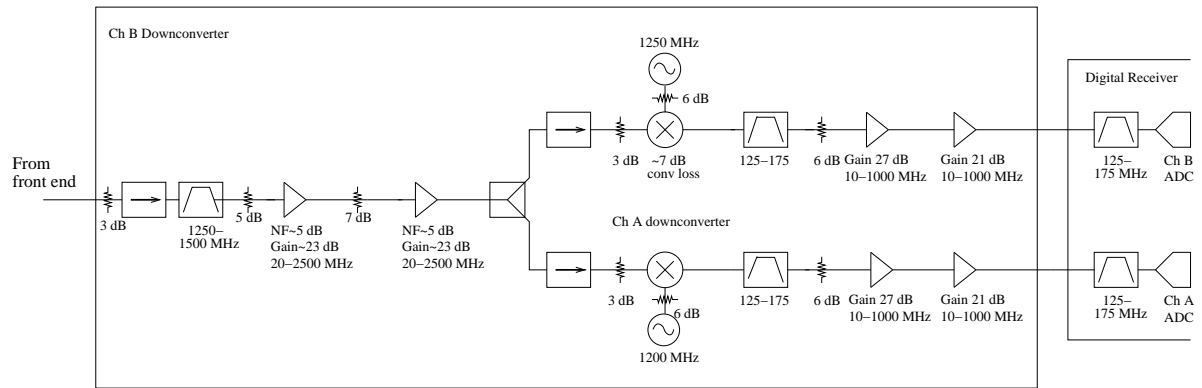
Figure 10: Block diagram of downconversion unit developed for pool observations

Figure 11: Photograph of antenna deployed on ElectroScience Laboratory roof

6.2.2 Thermal control systems

In addition, a thermal control and measurement system was developed for the front-end unit, in order to enhance system gain stability as well as to provide accurate control of internal calibration load noise powers. A commercial thermal control unit was purchased for use with a thermo-electric cooling element mounted in the front-end enclosure [67]. A custom temperature monitoring circuit was designed and developed [68]-[69] as well due to difficulty in locating a highly accurate temperature sensor (i.e. accurate within 0.1 K) for the system. Tests showed these systems to perform adequately at keeping the front end average temperature stable to within approximately 0.2 K over long periods of time. One issue was encountered involving cross-talk between the pulse-width modulated TEC power lines and the temperature monitoring circuit. However these effects could be mitigated simply by averaging recorded temperatures over several measurements.

6.2.3 Results

Experiments began September 2003; Figure 12 includes photographs of the water pool when uncovered, when covered with absorbing loads (the "hot" calibration target) and when covered with reflectors (the "cold" calibration target). The campaign again focused on comparing calibrated integrated brightnesses with the APB either on or off. A calibration cycle, requiring covering the water pool with the absorbers, then reflectors, then uncovered pool observations, could be completed in approximately 40 minutes. The physical temperature of the water pool was monitored during these experiments, as well as that of the ground surrounding the water pool.

Unfortunately, calibrated pool brightnesses obtained from these measurements consistently showed large variations (up to 20-30 K) with frequency in the 1325-1425 MHz band. Such variations are not expected from a water pool target, whose brightness should remain within 1-2 K over this frequency range. Sample results from these campaigns are provided in [21]-[23]. The experiments were repeated several times during the period Sept 2003 to Feb 2004 (hampered substantially by the Winter of 2004), but similar problems were found to appear (with differing frequency varia-
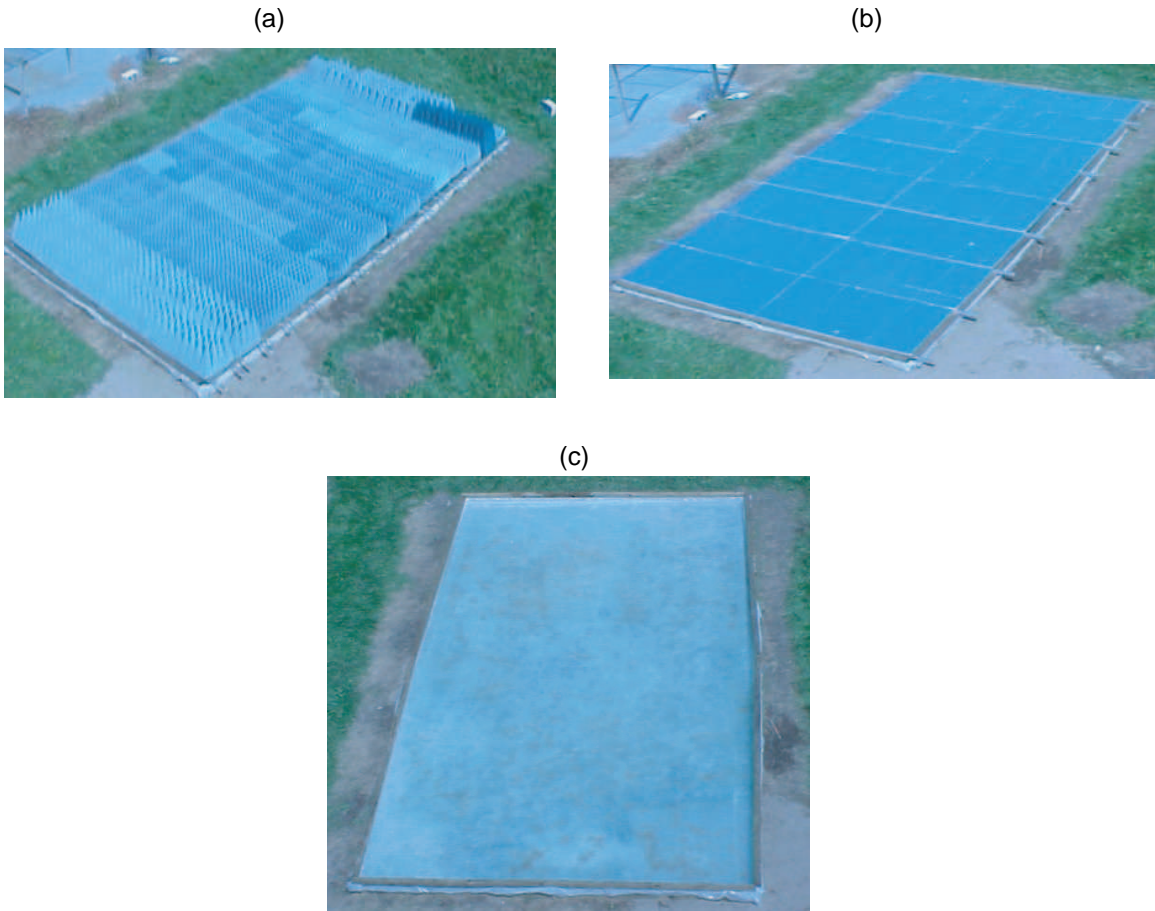
(a)

(b)

(c)

Figure 12: Water pool (a) covered with absorber (b) covered with reflecting material, and (c) uncovered

tions) in each measurement. Modifications of the front-end and downconverter stages performed during this time period yielded no improvement in the calibrated data. Results qualitatively continued to show the impact of the APB on removing the local ARSR influence, and the higher sensitivity obtained due to even an inaccurate calibration revealed the presence of several narrowband interferers within the band of interest.

Analysis of relative power variations observed during the period of an experiment made clear that significant changes in the received power (not uniform across frequency and not identical across all switch ports) were occurring during the period of the measurement. Unfortunately, the configuration of this experiment made separation of internal hardware issues from possible external RFI and/or environmental variations difficult. For this reason an alternate experimental campaign was initiated beginning in Spring 2004. Note LISR3 prototype development efforts continued independent of this campaign throughout late 2003 and 2004.

6.3 LISR2/3 Sky observations

6.3.1 Original tests

To address the possible impact of antenna noise contributions from regions outside the area of the pool target previously used, it was decided to utilize up-ward looking sky observations. Because reaching the far-field is not an issue for sky observations, a much more directive antenna can be used, resulting in reduced contributions from surrounding ground, building, and other environmental noise. Accordingly, a 3 m reflector antenna located in front of the ElectroScience Laboratory was employed, with two distinct feed systems. The first feed used was in existence from prior measurements with this antenna, but did not include a front end with any internal calibration loads or thermal control. First tests were performed using the existing feed in late Spring 2004. Results again quantitatively showed APB effectiveness, but continued to show significant gain variations with time, likely due to the limitations of the previous frontend.

31

Even with these issues, tests showed the system's ability to observe astronomical sources, including the moon and hydrogen line emissions from the galactic center. Figure 13 plots relative power variations observed near the 1420.4 MHz hydrogen emission line frequency over a 24 hour period. The "S" shaped curve observed captures the Doppler shift of the hydrogen line as differing portions of galactic emission are observed. The wider emission feature around hour 6 is associated with observations near the galactic center, while the broad increase around hour 14 is associated with the moon entering the antenna pattern. Note these measurements were obtained at extremely high spectral resolution through use of the radiometer "capture" mode: the 256K sample capture (i.e. 2.6 msec of data sampled at 10 nsec) makes possible results in spectral resolutions 256 times narrower than those of the standard system output. Such high spectral resolution is needed to resolve the hydrogen line Doppler shift. The presence of such sources in sky observations clearly suggests the possibility of a calibration procedure based on the expected brightnesses of such sources. In general, it is expected that the sky provides a slowly varying brightness comprised of known cosmic background, atmospheric, and astronomical source contributions [42]. If a high degree of stability of the system can be demonstrated, sky observations over long time periods should show only a slow evolution as various astronomical sources enter the antenna pattern, while more rapid brightness variations would indicate RFI effects. Overall the goal of the sky observation campaign is to demonstrate reduction of RFI effects, including calibrated information on the number of Kelvins of RFI reduction achieved.

6.3.2 Sky observations with IIP feed

Efforts to replace the previous front end with the feed/front-end used in the pool campaign were begun late Spring 2004, with first observations occurring in Summer 2004. Figure 14 is a photograph of the feed mounted on the antenna. Several tests were performed through Fall 2004-Spring 2005 to investigate system performance. One issue involves angular alignment of the antenna for viewing particular astronomical sources; experiments based on observation of the Sun over several days were used to improve
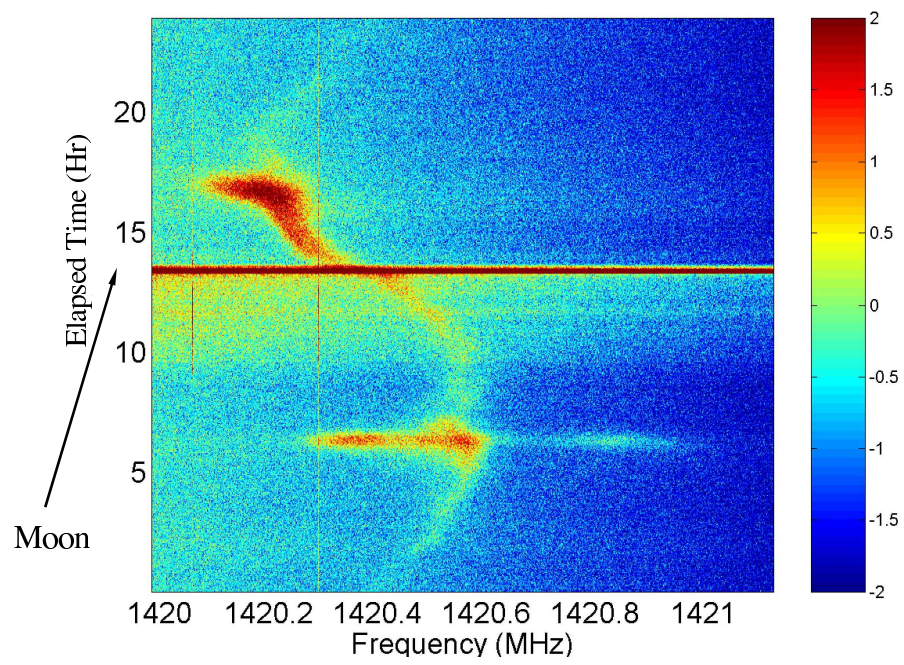
Figure 13: Relative power variations observed with original 3-m feed near the Hydrogen line frequency

understanding of the antenna alignment and gain pattern. Relative power variations were found to have improved compared to the previous feed system, but significant variations (non-uniform in frequency) continued to occur that did not appear related to RFI sources. Work to identify these variations suggested some temperature instabilities in the downconverter module (previously not temperature controlled) as well as possible cross-talk of front end noise after the LNA being received by the antenna. Modifications to address these problems (including incorporating temperature control of the downconverter stage) were completed by Spring 2005. Unfortunately, the problems encountered have delayed astronomical observations, and as of the time of this report, a completely calibrated dataset at L-band has not been achieved. However system stability has greatly improved, and it appears that such a dataset will be possible in the near future.
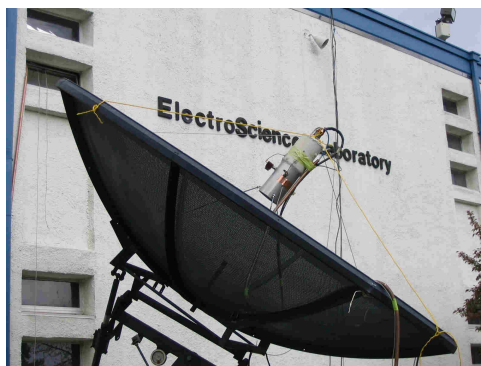
Figure 14: 3-m diameter parabolic reflector and feed/front-end

As an example, Figure 15 illustrates relative power variations in power spectra over 7 hours of observations (00:00 - 7:15am, local time). The color scale represents -0.1 dB to 0.1 dB, so that small variations in relative power levels are illustrated; results staying within these limits over several hours indicate a highly stable system. Plots are normalized by their average over time before conversion to decibels, and results are presented in terms of power spectra (i.e. power outputs of the 1024 point FFT) integrated over 5.3 seconds.

Figure 15-a is the raw noise power of vertically polarized antenna port, with the blanker turned off. Results show a relatively stable behavior, although some long

term trends in the relative power across all frequencies are observed, indicating slow variations in the receiver gain. Vertical "streaks" in the figure indicate the presence of frequency localized RFI, where the power varies significantly more than in the RFI-free bins. Strong interferers are observed near 1330 MHz (the ARSR system), 1400 MHz, 1403 MHz, and other frequencies.

Figure 15-b provides a similar plot, but results are illustrated with the blanker turned on. A dramatic reduction in the 1330 MHz source is observed; other non-pulsed RFI sources are not significantly affected.

Figure 15-c plots the results of Figure 15-b in terms of relative power variations after an internal calibration procedure using the noise diode and terminator standards is applied. The long term trends observed in plots (a) and (b) are reduced, indicating that the gain variations observed affect the terminator and noise diode sources in a manner similar to the antenna ports. Some problems in the correction are observed at the band edges and in the cross-over region (1370-1380 MHz) between the two channels, but system stability is otherwise improved through the internal calibration procedure. Efforts to improve these procedures are continuing.

Figure 16 plots relative variations in time of the total power of Figure 15-c. The results were computed from the sum of all frequency channels, with the exception of frequencies near 1400 MHz and 1403 MHz since these bands contain strong narrow-band RFI. Results show total power variations within 0.05 dB over 7 hours of observations. The increase in power observed (the results presented have a negative gain due to the internal calibration procedure) seen at 6:30am corresponds to observation of the galactic plane. The internal calibration procedure (data not shown) shows these variations to be on the order of a few Kelvin. Further processing of these data to exclude other narrowband RFI sources should provide additional information and/or stability, and will continue until a final result is achieved.
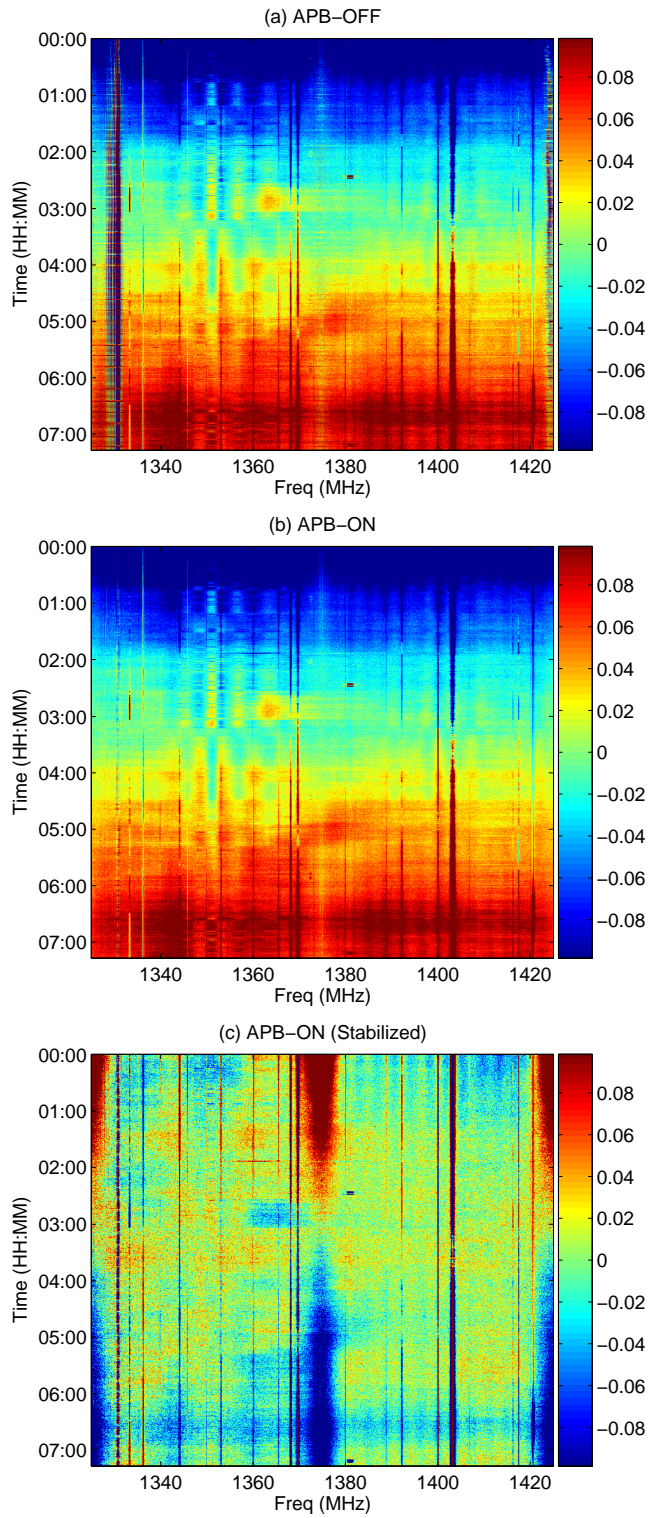
Figure 15: Relative power in dB, 7-hrs observation, V-Pol antenna port. The antenna was fixed at azimuth angle=154°, polar angle=26.5° (from zenith)
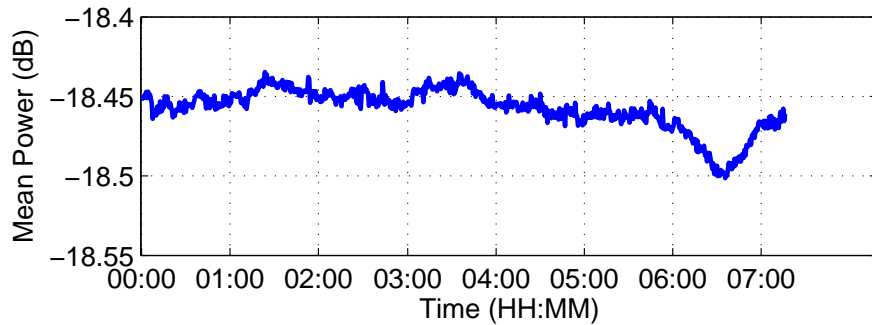
Figure 16: Relative variations of the internally calibrated total power (i.e. integrated over frequency) in Figure 15-c.

6.4 CISR airborne measurements

6.4.1 CISR system design

Though the IIP project focuses on L-band applications, the digital receiver backend developed can be used at other RF frequencies. C-band is another RF frequency of particular concern for RFI corruption, as this band is desirable for soil moisture and sea surface temperature sensing, while there is no protected spectrum available. Recent airborne [70] and satellite data [71] clearly shows RFI corruption of satellite measured data (using the "traditional" radiometer designs described in Section 3.) Due to concerns over RFI at C-band as well as current development of the Conical Microwave Imager/Sounder (CMIS) radiometer as part of the National Polar-Orbiting Environmental Satellite System (NPOESS), a project was initiated in August of 2003 to investigate C-band RFI under NPOESS support. In this project, the LISR2 digital backend was operated in conjunction with the Polar Scanning Radiometer (PSR) system of NOAA/ETL [72]. Antenna, front-end, and downconversion stages were provided by the PSR, while the LISR2 backend provides high temporal and spectral resolution RFI observation and mitigation. The complete system was renamed the C-band Interference Suppressing Radiometer (CISR); see [16] for additional information on the combined system.

6.4.2 CISR 2004 deployments

CISR was deployed initially in the Soil Moisture Experiment 2004 (August), but problems with the aircraft as well as with the downconversion and backend implementations resulted in only minimal data being obtained. A larger dataset was obtained during a test flight on October 8th, 2004 in the Chesapeake bay region. Analysis of the data under NPOESS support has shown numerous RFI sources encountered, including both pulsed and more continuous emitters [73]. Because the PSR traditional radiometer system (operated simultaneously with digital backend observations) includes 4 analog sub-channels, this dataset provides an opportunity for evaluating RFI mitigation performance of an analog sub-band approach versus mitigation with the much higher spectral and temporal resolution digital data. Results show that the analog sub-band approach often yields apparently reasonable RFI suppression in cases where one of the sub-bands is RFI-free, but incomplete removal of RFI when all sub-bands contain RFI. This situation is encountered several times in the measured dataset. Digital backend data on the other hand provide sufficient spectral resolution to identify and remove RFI even in these cases.

6.4.3 CISR sample results

The calibration procedure of the PSR front end enables a calibration of the digital backend dataset to be performed. However the tuning process utilized to provide complete observations of 5.5 to 7.7 GHz at C-band [16],[73], as well as the use of several digital backend modes during the flights, complicates the process and results in calibration for only a subset of the measured data. An result demonstrating spectral RFI removal is provided in Figure 17, which plots calibrated brightnesses recorded by the 4 PSR analog sub-band channels during an over-water portion of the October 8th, 2004 flight. These 4 sub-bands correspond to $5.8 - 6.2$, $6.3 - 6.7$, $6.75 - 7.1$, and $7.15 - 7.5$ GHz, respectively, and remain large bandwidth (approx 400 MHz) channels. Figure 17 also includes results after an RFI removal algorithm [70] is applied to these 4 sub-bands; the algorithm is based on the assumption that the 4 subband brightnesses should be well-fit by a line in frequency. Brightnesses that violate this
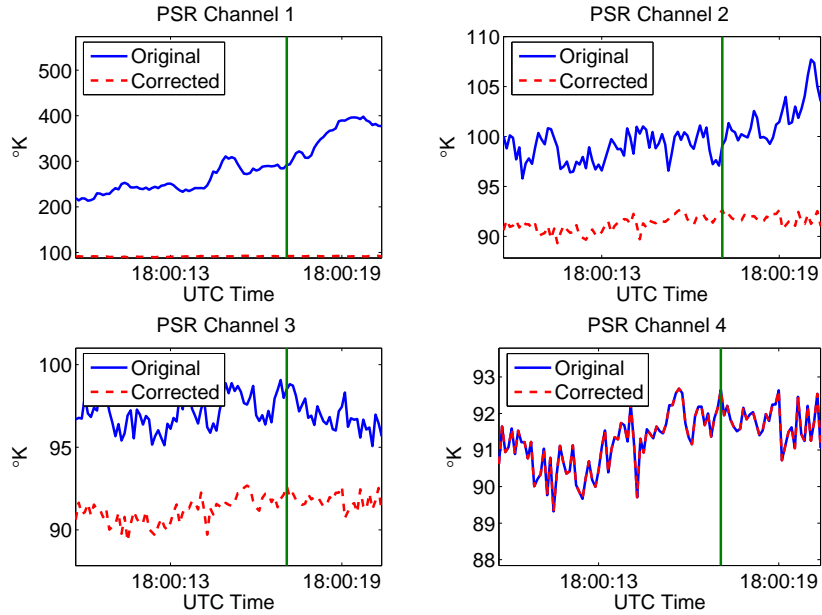
Figure 17: PSR measured brightnesses versus time during a portion of the October 8th, 2004 test flight. Brightnesses in 4 PSR analog sub-bands are plotted before and after a 4 sub-band RFI removal process [70] is applied.

assumption are deemed corrupted, and replaced with values from channels that are deemed acceptable. This procedure is found to be effective in removing obvious RFI contributions in Figure 17; note that channel four however is not modified, as this channel typically produces the smallest brightnesses throughout this portion of the flight.

The vertical line in Figure 17 marks a particular point where calibrated digital backend data is available within the bandwidth of PSR channel 4. Figure 18 plots calibrated CISR brightnesses at this point, and shows the presence of a strong narrowband source near 7110 MHz. Note data within a few MHz of the CISR band-edges are not reliably calibrated due to reduced gain in the IF passband, and are excluded in the following discussion. Though not shown, data with the APB on showed no impact on this source, indicating this source's slow variation in time. Mean brightnesses for this CISR spectrum were compared to those excluding the RFI region marked between the two vertical lines in Figure 18. Results showed this source to contribute approximately 4 K when scaled to the PSR channel 4 bandwidth. This
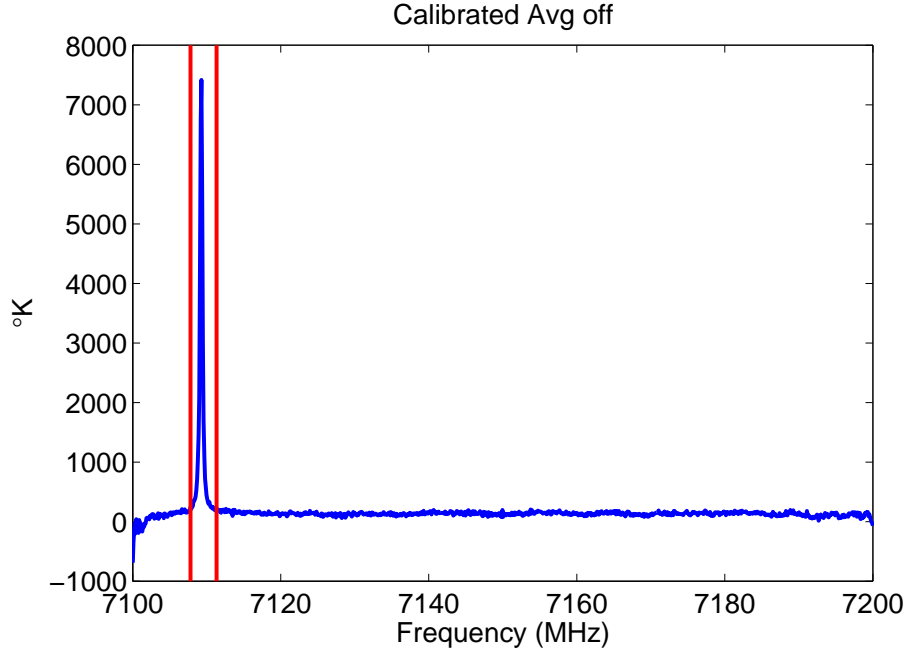
Figure 18: Calibrated CISR (i.e. digital backend) brightnesses (APB off) measured at the location of the vertical line in Figure 17

level of contribution is consistent when comparing the channel 4 data of Figure 17 to sea observations earlier in time. This example clearly demonstrates the advantages of higher spectral resolution in removing RFI, as this narrowband source clearly identifiable as RFI (i.e. brightness greater than 7000 K) in the digital data produces a low-level RFI contribution (i.e. 4 K) to a large bandwidth channel that is much more difficult to separate from geophysical variations.

C-band observations will continue in 2005 under NPOESS support; a journal article documenting results from the October 8th flight is currently in preparation. Efforts to match the observed RFI sources against licensed C-band sources from an NPOESS database [74] have also been initiated to assess analytical methods for forecasting RFI levels from such database information.

7 Deployment in space

Given the results of the project, an exit TRL level of between 4 and 5 is deemed reasonable. TRL 5 could be considered achieved if completely calibrated L-band

data were obtained; the calibrated C-band data illustrated provides some TRL 5 contributions at the conclusion of the project (April 2005).

Extending this technology to TRL 6 for use in space involves a few issues that must be addressed, including hardware availability, alternate designs, data rate issues, and appropriate algorithm choices. These topics are discussed below.

7.1 Hardware issues

With regard to system hardware, a space-based L-band system employing these technologies would be identical to a space-based system without these technologies in terms of the basic antenna and front-end configuration. Inclusion of a downconverter would increase the amount of required RF hardware, and could possibly be avoided through use of direct sampling systems. Such a choice requires consideration of currently available ADC parts that can be deployed in space. A review of the literature [75]-[76] shows that ADC's similar to those used in the IIP system are already being used in space, and rad-tolerant parts operating at 200 MSPS are available currently. However, requiring such parts to be used in a direct sampling system is likely to produce higher risk than including analog downconversion components. For this reason it is recommended that the downconversion stage be retained in initial designs of space systems.

The use of FPGA's (i.e. reconfigurable) or more static (i.e. ASIC) digital components for an RFI removal processor in space deserves consideration. The flexibility of FPGA components however combined with the difficulty of completely forecasting the RFI to be experienced from space observations clearly motivates use of FPGA's if possible. For satellite systems which must be designed several years before launch and then continued for an additional several years in operations, the ability to modify the RFI suppression techniques used is extremely valuable; fixed algorithms on an ASIC component have a strong probability of becoming obsolete should the RFI environment change significantly.

Of course, the availability of space qualified FPGA's of sufficient size and speed is an important issue if FPGA's are to be used. It is important to distinguish between

"rad-hard" and "rad-tolerant" components in this discussion. "Rad-hard" components can survive extremely large radiation doses with extremely low rates of single event failures, while "rad-tolerant" components experience somewhat higher rates of single event failures. However, for FPGA systems, programming methods exist to incorporate circuit redundancies as well as continual reprogramming so that single event effects can be dramatically reduced. See [77] for a detailed report on the use of FPGA's in space and a discussion of radiation failure reduction techniques. This reference also shows that rad-tolerant FPGA's of similar size and speed to those used in LISR2 are currently available. Similar FPGA's are already being used in space applications. It appears that FPGA technological limitations for space deployment have already been overcome as of the completion of the project, and continued innovations [78] are increasing capabilities beyond those used in this project.

In summary, the component technology (i.e. ADC's and FPGA's) required to implement a digital backend for space based microwave radiometers appears to be available at the present time.

7.2   System design and algorithm issues

A second issue is related to the basic architecture to be utilized for a space-based RFI removal processor, as well as choice of specific RFI removal algorithms.

7.2.1   Temporal blanking

The studies of this project have shown that temporal pulse removal can be extremely effective against radar sources, particularly by removing any dynamic range issues caused in later digital processing. If radar (or other pulsed) sources are expected to occur within the bandwidth of interest, the temporal blanking algorithm developed appears highly relevant.

At L-band, even if operation within the protected 1400-1427 MHz spectrum is planned, the possibility remains that strong radar sources at frequencies up to 1350 MHz could leak through any filter response and still produce observable RFI. Note if only the protected spectrum were digitized, such radar leakage would be aliased to lie

42

within the band of interest when digitized. The possibility of digitizing a bandwidth larger than that of the protected spectrum (even after a hard analog filter limits the analog bandwidth to the protected band) should be considered if it is desired to avoid such leakage. In either case, retaining temporal blanking as a first stage in RFI-removal deserves strong consideration for the removal of radar effects. Pulse blanking also reduces the need for rapid temporal sampling of the final data stream (i.e. through a satellite downlink), since the algorithm should remove the majority of likely short-time duration RFI.

7.2.2 Frequency domain processing

With regard to frequency domain RFI removal, two strategies regarding the generation of sub-channel results are apparent. The first utilizes the FFT approach of the current project, and thereby is capable of generating a large number of sub-channels within a reasonable fraction of available FPGA hardware. The FFT however can experience some corruption of the signal spectrum due to "edge effects" associated with discontinuities along boundaries of the FFT frames. Such effects can be reduced through the use of appropriate windows. The FFT also produces an output data rate reduced by the length of the FFT frame. Appropriate dynamic range issues must be addressed as well, as the FFT is inherently a floating point operation, while FPGA programming is simplified if fixed-point arithmetic is used exclusively. The design utilized in the IIP prototype [36]-[39] appears to address these issues satisfactorily, and the studies of the project show that spectrum distortion effects due to partially-blanked frames appear manageable.

An alternate approach is based on the use of a digital filter (likely a finite impulse response (FIR) filter) for each digital sub-channel. Such an approach requires additional digital hardware as more channels are added, with the hardware size likely exceeding that of the FFT approach as the number of channels increases. Retaining fixed point arithmetic in digital filters is simpler, and the output data rate is not reduced compared to that of the input. However the averaging operations inherent in filtering reduce the bandwidth of the output signal, so that resampling to a lower

sample rate may be appropriate. Because no frame boundaries are introduced, frame edge discontinuities are not implicitly involved in this case. However, signal discontinuities caused by the presence of large interferers or transitions in the blanking operation still distort filter outputs during the averaging time of the filter.

The choice of either approach likely depends on the spectral resolution desired in removing RFI for a space-based system. If a low spectral resolution is deemed acceptable (or when used with a receiver sampling a small RF bandwidth), the FIR approach may be preferable. However, the known small bandwidths of many RFI sources near L-band (typically less than 1 MHz) make high spectral resolution desirable when possible. Based on project results, it is recommended that a spectral resolution finer than 1 MHz be utilized either through FIR or FFT techniques. The choice of either an FIR or FFT approach will require detailed information on the FPGA component to be utilized as well as the ultimate RF bandwidth to be sampled.

7.2.3 Other RFI removal algorithms

Efforts of the IIP project have focused on simple time- and frequency-domain RFI removal operations. These techniques appear to be acceptable for the majority of the sources encountered during the course of the project, representing cases where sources occupy only a fraction of the available radiometer integration time and/or bandwidth. However, in cases where sources may occupy large regions of both time and frequency, the performance of these approaches should be expected to degrade. The desire of communication systems to increase the amount of information within a fixed bandwidth by occupying as much of the time-frequency space as possible suggests that such sources are likely to increase in the future. Increasing plans for "ultra-wideband" communication systems, where low power levels are broadcast throughout a broad range of microwave frequencies, also suggest such sources may become more widespread in the future.

Mitigation of these sources will require research into more advanced algorithms. One technique for such sources involves incorporating a model of expected RFI signal properties into the detection and removal process. The model includes a set of pa-

rameters (for example, amplitude, phase, symbol information, etc.) that is fit to the incoming data (ultimately in real-time), then this modeled data is subtracted from the data stream to remove RFI. Such an approach has been demonstrated with RFI from the GLONASS navigational satellite downlink [79]. However such algorithms are more complex than simple time- and frequency-blanking, and will require additional research to develop an efficient hardware implementation.

A related algorithm proposed by Prof. C. Ruf of the University of Michigan (see Section 7.3) involves histogram analysis of received data. As RFI-free data should be expected to follow a Gaussian distribution when integrated over short integration periods, any deviation from Gaussianity can indicate the presence of RFI. One test of the histograms can be performed through computation of histogram moments. Implementation of this approach in hardware appears straight-forward, although the methods sensitivity to low-level RFI will need to be carefully examined. See Section 7.3 for additional discussion of investigation of alternative RFI mitigation algorithms.

7.2.4 Data rate issues

Related to the number of sub-channels retained, the final system data rate is also an important factor for space designs. As discussed previously, the primary issue involves whether cross-frequency blanking should be done on-board, with only a single channel, RFI processed brightness ultimately downlinked, or whether all sub-channels should be downlinked for RFI cross-frequency post-processing. Although the use of FPGA's can retain flexibility in spectral RFI removal processing, applying such algorithms in post-processing remains the most desirable option, particularly for the first systems deployed.

The current LISR prototypes obtain a datarate 1024 times that of a typical radiometer; this rate is likely to be unmanageable for a space-based system. A smaller number of channels (perhaps 16 to 64) would likely be acceptable. A hybrid approach could be utilized wherein an on-board processor removes RFI at a higher spectral resolution and outputs data at reduced, but still fine, spectral resolution.

It is highly recommended that multiple frequency sub-bands be employed in future systems, regardless of the technique utilized for generating these sub-bands.

7.3 Alternate designs: proposal for HYDROS

To continue the research begun under this project for applications at L-band, a proposal to the 2004 NASA IIP program was developed in conjunction with Prof. C. Ruf from the University of Michigan and Dr. Jeffrey Piepmeier of NASA GSFC. In this proposal, the digital backends of the project will be employed in continued ground- and aircraft based studies in order to clarify further RFI removal performance in realistic environments (TRL 5). An alternate digital backend developed by Prof. Ruf, as well as a more analog system developed by Dr. Piepmeier will be included in these measurements to cross-assess the performance of each receiver. The system employed by Prof. Ruf is similar in concept to the IIP receiver, but uses an RFI removal algorithm based on a histogram analysis of the received power within FIR generated sub-channels.

Based on the results of these comparisons, a complete digital backend design will be developed for the L-band HYDROS radiometer [80]. The HYDROS mission team has expressed an interest in possible inclusion of such a digital backend in the HYDROS instrument. Such an effort would clearly produce TRL 6 results for space deployment. Therefore extension of the technologies developed under the IIP project to TRL 6 can be estimated as feasible within the time frame of 2-3 years (the period of the proposed project.) The recent announcement of the success of the joint proposal assures that these efforts will continue.

8 Conclusions

Under the support of the NASA IIP program, The Ohio State University, in cooperation of Dr. S. W. Ellingson of Virginia Tech, has demonstrated the potential for RFI mitigation in space-borne radiometers through the use of digital receiver backends. Results from the project have qualitatively shown the gains that can be achieved through simple temporal and spectral RFI removal techniques. Results from

project design efforts, RFI surveys, prototype demonstrations, and air-based observations have been described in this report, as well as a summary of issues for space deployment.

It is certain that incorporation of digital receiver technologies into passive remote sensing systems will increase in the future, as such technologies can dramatically improve the capabilities of such systems in mitigating RFI. Other advantages of these systems not explicitly discussed here include potential stability improvements, possible calibration enhancements, as well as more simple and accurate computation of correlations in either polarimetric or interferometric sensors. Evaluation of these gains awaits further studies and the first deployment of these systems in space.

References

[1] J. T. Johnson and S. W. Ellingson, "Digital Receiver with Interference Suppression for Microwave Radiometry", project proposal, available at `http://esl.eng.ohio-state.edu/~rstheory/iip/docserv.html`, 2001.

[2] NPOESS IGS project DG133E-04-CN-0049, "Demonstration of RFI suppressing radiometry at C-band," project proposal, 2003. (available at `http://www.ece.osu.edu/~johnson/cisr`)

[3] C. Ruf, J. T. Johnson, and J. Piepmeier, "Development of an agile digital detector for RFI detection and Mitigation on spaceborne radiometers," proposal submitted to the 2004 NASA IIP program.

[4] N. Niamsuwan, M. S. Thesis, The Ohio State University, to be completed June 2005.

[5] S. W. Ellingson and G. A. Hampson, "Mitigation of radar interference in L-band radio astronomy," *Astr. Journal Suppl. Ser.,* vol. 147, pp. 167-176, 2003.

[6] N. Niamsuwan, J. T. Johnson, and S. W. Ellingson, "Examination of a simple pulse blanking technique for RFI mitigation" accepted by *Radio Science,* 2004.

[7] S. W. Ellingson, G. A. Hampson, and J. T. Johnson, "Characterization of L-band RFI and implications for mitigation techniques," *IEEE Geoscience and Remote Sensing Symposium,* conference proceedings, 2003.

[8] S. W. Ellingson, G. A. Hampson, and J. T. Johnson, "Design of an L-band microwave radiometer with active mitigation of interference," *IEEE Geoscience and Remote Sensing Symposium,* conference proceedings, 2003.

[9] G. A. Hampson, S. W. Ellingson, and J. T. Johnson, "Design of an L-band microwave radiometer with active mitigation of interference," *IEEE Antennas and Propagation/URSI Symposium,* conference proceedings, 2003.

[10] S. W. Ellingson, G. A. Hampson, and J. T. Johnson, "Design of an L-band microwave radiometer with active mitigation of interference," *NASA Earth Science Technology Conference,* conference proceedings, 2003.

[11] G. A. Hampson, S. W. Ellingson, and J. T. Johnson, "Design and demonstration of an interference suppressing microwave radiometer," *IEEE Aerospace Conference,* conference proceedings, 2004.

[12] J. T. Johnson, G. A. Hampson, and S. W. Ellingson, "Design and demonstration of an interference suppressing microwave radiometer," *IEEE Geoscience and Remote Sensing Symposium,* conference proceedings, 2004.

[13] N. Niamsuwan, J. T. Johnson, and S. W. Ellingson, "Examination of a simple pulse blanking technique for RFI mitigation," *Workshop in Mitigation of Radio Frequency Interference in Radio Astronomy,* conference proceedings, 2004.

[14] N. Niamsuwan and J. T. Johnson, "Sky observations at L-band using an interference suppressing radiometer," *IEEE Geoscience and Remote Sensing Symposium,* conference proceedings, 2005.

[15] S. W. Ellingson, G. A. Hampson, and J. T. Johnson, "Digital receiver with interference suppression for microwave radiometry," NASA Tech Brief GSC14776-1, Feb 2005.

[16] J. T. Johnson, A. J. Gasiewski, G. A. Hampson, S. W. Ellingson, R. Krishnamarachi, and M. Klein, "Airborne radio frequency interference studies at C-band using a digital receiver," *IEEE Geoscience and Remote Sensing Symposium,* paper in conference proceedings, 2004. (available at `http://www.ece.osu.edu/`
`~johnson/cisr`)

[17] IIP project document server, `http://esl.eng.ohio-state.edu/~rstheory/iip/`
`docserv.html`, July 10, 2002.

[18] J. T. Johnson and S. W. Ellingson, Year 1 Interim Review Presentation, available at `http://esl.eng.ohio-state.edu/~rstheory/iip/docserv.html`, July 10, 2002.

[19] J. T. Johnson, S. W. Ellingson, and G. A. Hampson, Year 1 Annual Review Presentation, available at `http://esl.eng.ohio-state.edu/~rstheory/iip/docserv.html`, Oct 4, 2002.

[20] J. T. Johnson, S. W. Ellingson, G. A. Hampson, and N. Niltawach, Year 2 Interim Review Presentation, available at `http://esl.eng.ohio-state.edu/~rstheory/iip/docserv.html`, April 29, 2003.

[21] J. T. Johnson, S. W. Ellingson, and G. A. Hampson, Year 2 Annual Review Presentation, available at `http://esl.eng.ohio-state.edu/~rstheory/iip/docserv.html`, Oct 28, 2003.

[22] J. T. Johnson, S. W. Ellingson, and G. A. Hampson, Year 3 Interim Review Presentation, available at `http://esl.eng.ohio-state.edu/~rstheory/iip/docserv.html`, May 13, 2004.

[23] J. T. Johnson, N. Niamsuwan, B. Guner, and S. W. Ellingson, Year 3 Annual Review Presentation, available at `http://esl.eng.ohio-state.edu/~rstheory/iip/docserv.html`, April 19th, 2005.

[24] Fischman, M. A. and A. W. England, "Sensitivity of a 1.4 GHz direct-sampling digital radiometer," *IEEE Trans. Geosc. Rem. Sens.* , vol. 37, pp. 2172–2180, 1999.

[25] S. W. Ellingson, "A Design Concept for the IIP Radiometer," project internal report, available at `http://esl.eng.ohio-state.edu/~rstheory/iip/docserv.html`, January 11, 2002.

[26] S. W. Ellingson, "Design Concept for the IIP Radiometer RFI Processor," project internal report, available at `http://esl.eng.ohio-state.edu/~rstheory/iip/docserv.html`, January 23, 2002.

[27] S. W. Ellingson, "A Survey of A/Ds Which Sample Greater than 100 MSPS with Power Consumption Less Than 1W," January 15, 2002.

[28] G. A. Hampson, "AD9054 Prototype Evaluation," project internal report, available at `http://esl.eng.ohio-state.edu/~rstheory/iip/docserv.html`, March 5, 2002.

[29] G. A. Hampson, "AD9410 Prototype Evaluation,", project internal report, available at `http://esl.eng.ohio-state.edu/~rstheory/iip/docserv.html`, May 13, 2002.

[30] S. W. Ellingson, "Design of the IIP Radiometer Digital IF Section (Rev. 1)," project internal report, available at `http://esl.eng.ohio-state.edu/~rstheory/iip/docserv.html`, May 6, 2002.

[31] G. A. Hampson, "An FPGA Implementation of the Digital IF Processor,", project internal report, available at `http://esl.eng.ohio-state.edu/~rstheory/iip/docserv.html`, March 7, 2002.

[32] G. A. Hampson, "Implementation Results of the Digital IF Processor,", project internal report, available at `http://esl.eng.ohio-state.edu/~rstheory/iip/docserv.html`, May 15, 2002.

[33] S. W. Ellingson, "Functional Design of the Asynchronous Pulse Blanker (Rev. 1)," project internal report, available at `http://esl.eng.ohio-state.edu/~rstheory/iip/docserv.html`, May 1, 2002.

[34] G. A. Hampson, "Implementation of the Asynchronous Pulse Blanker,", project internal report, available at `http://esl.eng.ohio-state.edu/~rstheory/iip/docserv.html`, June 26, 2002.

[35] Ellingson, S. W., *Characterization of Some L-Band Signals Visible at Arecibo*, Technical Report 743467-2,The Ohio State University ElectroScience Laboratory, February 2003.

[36] G. A. Hampson, "A Possible 100 MSPS Altera FPGA FFT Processor," project internal report, available at `http://esl.eng.ohio-state.edu/~rstheory/iip/docserv.html`, March 12, 2002.

[37] G. A. Hampson, "Implementation of a Single FFT Processor,", project internal report, available at `http://esl.eng.ohio-state.edu/~rstheory/iip/docserv.html`, July 3, 2002.

[38] G. A. Hampson, "Implementation Results of a Windowed FFT,", project internal report, available at `http://esl.eng.ohio-state.edu/~rstheory/iip/docserv.html`, July 12, 2002.

[39] G. A. Hampson, "A Post-FFT Power Estimator Implementation," project internal report, available at `http://esl.eng.ohio-state.edu/~rstheory/iip/docserv.html`, April 17, 2002.

[40] G. A. Hampson, "A Post-FFT Spectral Integration Processor: Implementation and Measurement Results," project internal report, available at `http://esl.eng.ohio-state.edu/~rstheory/iip/docserv.html`, Sep 20, 2002.

[41] G. A. Hampson, "A 256K @ 32-bit Capture Card for the IIP Radiometer," project internal report, available at `http://esl.eng.ohio-state.edu/~rstheory/iip/docserv.html`, May 10, 2002.

[42] D. M. LeVine and S. Abraham, "Galactic noise and passive microwave remote sensing from space at L-band," *IEEE Trans. Geosc. Rem. Sens.,* vol. 42, pp. 119-129, 2004.

[43] G. A. Hampson, "Development of a 200 MHz Clock Generation Module," project internal report, available at `http://esl.eng.ohio-state.edu/~rstheory/iip/docserv.html`, March 6, 2002.

[44] G. A. Hampson, "A Possible Dual Digital IF Processor Implementation," project internal report, available at `http://esl.eng.ohio-state.edu/~rstheory/iip/docserv.html`, Oct 1, 2002.

[45] S. W. Ellingson, "Estimating RFI Levels Due to Air Surveillance Radar," project internal report, available at `http://esl.eng.ohio-state.edu/~rstheory/iip/docserv.html`, February 14, 2002.

[46] S. W. Ellingson, "Preliminary RFI Survey for IIP,", project internal report, available at `http://esl.eng.ohio-state.edu/~rstheory/iip/docserv.html`, June 11, 2002.

[47] S. W. Ellingson, "IIP RFI Survey: Version 2,", project internal report, available at `http://esl.eng.ohio-state.edu/~rstheory/iip/docserv.html`, July 16, 2002.

[48] S. W. Ellingson, "A Survey of 1200-1800 MHz Using a Discone and a Spiral with the Argus Front End," project internal report, available at `http://esl.eng.ohio-state.edu/~rstheory/iip/docserv.html`, October 12, 2002.

[49] S. W. Ellingson, "Agilent Spectrum Analyzer Computer Control Demo", project internal report, available at `http://esl.eng.ohio-state.edu/~rstheory/iip/docserv.html`, June 6, 2002.

[50] S. W. Ellingson, "Mounting Instruments on NASA's P-3 Aircraft, project internal report, available at `http://esl.eng.ohio-state.edu/~rstheory/iip/docserv.html`, June 29, 2002.

[51] S. W. Ellingson, "LISA System Design", project internal report, available at `http://esl.eng.ohio-state.edu/~rstheory/iip/docserv.html`, Sep 15, 2002.

[52] S. W. Ellingson and J. T. Johnson, "An Installer's Guide to LISA", project internal report, available at `http://esl.eng.ohio-state.edu/~rstheory/iip/docserv.html`, Sep 19, 2002.

[53] S. W. Ellingson, "Initial LISA Measurements from the ESL Roof", project internal report, available at `http://esl.eng.ohio-state.edu/~rstheory/iip/docserv.html`, Sep 15, 2002.

[54] S. W. Ellingson, "LISA: L-Band Interference Surveyor/Analyzer", project internal report, available at `http://esl.eng.ohio-state.edu/~rstheory/iip/docserv.html`, Jan 15th, 2003.

[55] S. W. Ellingson and J. T. Johnson, "Airborne RFI Measurements over the Mid-Atlantic Coast using LISA", project internal report, available at `http://esl.eng.ohio-state.edu/~rstheory/iip/docserv.html`, Feb 10, 2003.

[56] J. T. Johnson and S. W. Ellingson, "Airborne RFI measurements using LISA during transit to and in the Wakasa Bay Campaign", project internal report, available at `http://esl.eng.ohio-state.edu/~rstheory/iip/docserv.html` , July 3rd, 2003.

[57] J. T. Johnson, "Initial External Experiment Plan for IIP Radiometer" , project internal report, available at `http://esl.eng.ohio-state.edu/~rstheory/iip/docserv.html`, March 15, 2002.

[58] S. W. Ellingson and G. A. Hampson, "On Air Test of the IIP Receiver Using Observations of an ATC Radar", project internal report, available at `http://esl.eng.ohio-state.edu/~rstheory/iip/docserv.html`, June 29, 2002.

[59] G. A. Hampson and S. W. Ellingson, "Demonstration of the ESL-IIP Radiometer's Asynchronous Pulse Blanker: Mitigation of an Air Traffic Control Radar," project internal report, available at `http://esl.eng.ohio-state.edu/~rstheory/iip/docserv.html`, July 26, 2002.

[60] S. W. Ellingson and G. A. Hampson, "RFI and Asynchronous Pulse Blanking at Arecibo," project internal report, available at `http://esl.eng.ohio-state.edu/~rstheory/iip/docserv.html`, Nov 12, 2002.

[61] J. T. Johnson, "Brightness Temperature of a Flat Water Surface" , project internal report, available at `http://esl.eng.ohio-state.edu/~rstheory/iip/docserv.html`, February 26, 2002.

[62] J. T. Johnson, "Continued External Experiment Plan for IIP Radiometer," project internal report, available at `http://esl.eng.ohio-state.edu/~rstheory/iip/docserv.html`, April 10, 2002.

[63] N. Niltawach and J. T. Johnson, "Reflector Antenna, its Mount and Microwave Absorbers for IIP Radiometer Experiments", project internal report, available at `http://esl.eng.ohio-state.edu/~rstheory/iip/docserv.html`, May 8, 2003.

[64] S. W. Ellingson, "Front End Version 1 Design", project internal report, available at `http://esl.eng.ohio-state.edu/~rstheory/iip/docserv.html`, February 22, 2002.

[65] S. W. Ellingson, "Front End Version 2 Design," project internal report, available at `http://esl.eng.ohio-state.edu/~rstheory/iip/docserv.html`, Sep 25, 2002.

[66] S. W. Ellingson, "A Simple Technique for Measuring Noise Figure,", project internal report, available at `http://esl.eng.ohio-state.edu/~rstheory/iip/docserv.html`, Sep 26, 2002.

[67] N. Niltawach and J. T. Johnson, "TEC and TEC Controller for Temperature Stabilized Plate," project internal report, available at `http://esl.eng.ohio-state.edu/~rstheory/iip/docserv.html`, May 15, 2003

[68] J. Johnson and G. Hampson, "Initial Plan for a Precision Temperature Sensor," project internal report, available at `http://esl.eng.ohio-state.edu/~rstheory/iip/docserv.html`, Sep 10, 2002.

[69] N. Niltawach, J. T. Johnson, and G. A. Hampson, "Implementation of a Temperature Monitoring Circuit," project internal report, available at `http://esl.eng.ohio-state.edu/~rstheory/iip/docserv.html`, May 6, 2003

[70] Gasiewski, A. J., M. Klein, A. Yevgrafov, and V. Leuski, "Interference mitigation in passive microwave radiometry," *IGARSS'02* conference proceedings, 2002.

[71] Ellingson, S. W. and J. T. Johnson, "A polarimetric survey of radio frequency interference in C- and X-bands in the continental United States using WindSAT radiometry," submitted to *IEEE Trans. Geosc. Rem. Sens.,* 2004.

[72] Polar Scanning Radiometer web site, `http://www.etl.noaa.gov/technology/psr` .

[73] "Airborne RFI measurements with PSR/CXI and CISR in the Chesapeake Bay Region: Initial Data Examination," project technical report, 2004. (available at `http://www.ece.osu.edu/~johnson/cisr`)

[74] Kunkee, D., Aerospace corporation, personal communication, 2005.

[75] "NASA/JPL A/D Converter Selection Guide," NASA report, available at `http://parts.jpl.nasa.gov/docs/adguide011405.pdf`, 2005. See also `http://parts.jpl.nasa.gov`.

[76] S. Agarwal, "Analog to digital converter evaluation for space applications," NASA report, available at `http://parts.jpl.nasa.gov/cots/internal/adc97.pdf`, 1997.

[77] B. Box, "A report on the use of FPGA's in space," project internal report, available at `http://esl.eng.ohio-state.edu/~rstheory/iip/docserv.html`, Aug 6, 2004.

[78] *2005 Military and Aerospace Programmable Logical Devices (MAPLD) International Conference,* at `http://klabs.org/mapld05/`. See also the Nasa office of Logic Design web site, `http://klabs.org/index.html`.

[79] S. W. Ellingson, J. Bunton, and J. F. Bell, "Removal of the GLONASS C/A signal from OH spectral line observations," *Astrophysical Jour. Suppl.,* vol. 135, pp. 87–93, 2001.

[80] HYDROS mission web site, `http://hydros.gsfc.nasa.gov` .